

REVISED RATES OF STELLAR DISRUPTION IN GALACTIC NUCLEI

JIANXIANG WANG AND DAVID MERRITT

Department of Physics and Astronomy, Rutgers University, New Brunswick, NJ 08903

Draft version October 30, 2018

ABSTRACT

We compute rates of tidal disruption of stars by supermassive black holes in galactic nuclei, using downwardly revised black hole masses from the $M_\bullet - \sigma$ relation. In galaxies with steep nuclear density profiles, which dominate the overall event rate, the disruption frequency varies inversely with assumed black hole mass. We compute a total rate for non-dwarf galaxies of $\sim 10^{-5} \text{ yr}^{-1} \text{ Mpc}^{-3}$, about a factor ten higher than in earlier studies. Disruption rates are predicted to be highest in nucleated dwarf galaxies, assuming that such galaxies contain black holes. Monitoring of a rich galaxy cluster for a few years could rule out the existence of intermediate mass black holes in dwarf galaxies.

Keywords: galaxies: elliptical and lenticular — galaxies: structure — galaxies: nuclei — stellar dynamics

1. INTRODUCTION

Stars that pass sufficiently close to a supermassive black hole will be tidally disrupted (Hills 1975, Frank & Rees 1976, Lidskii & Ozernoi 1979). Disruption of solar-type stars occurs at a distance $r_t \approx \mathcal{R}_\odot (M_\bullet / M_\odot)^{1/3}$, with M_\bullet the black hole mass; for $M_\bullet \lesssim 10^8 M_\odot$, the tidal radius lies beyond the black hole’s event horizon and disruption results in an energetic flare as the bound stellar debris falls back onto the black hole. Emission from the debris is expected to peak in the soft X-ray or UV domains, to have a maximum luminosity of $\sim 10^{44} \text{ erg s}^{-1} \approx 10^{11} \mathcal{L}_\odot$, and to decay on a time scale of weeks to months (Rees 1988, Evans & Kochanek 1989, Ulmer 1999, Kim, Park & Lee 1999). Detection of flares would constitute robust proof of the existence of supermassive black holes and could conceivably allow constraints to be placed on black hole masses and spins (Rees 1998).

The *ROSAT* All-Sky Survey detected soft X-ray outbursts from a number of galaxies with no previous history of Seyfert activity. Roughly half a dozen of these events had the properties of a tidal disruption flare (Komossa 2002 and references therein), and follow-up optical spectroscopy of the candidate galaxies confirmed that at least two were subsequently inactive (Gezari et al. 2003).

The mean event rate inferred from these outbursts is roughly consistent with theoretical predictions (Donley et al. 2002). Detailed calculations of the tidal disruption rate in samples of nearby galaxies have been published by Syer & Ulmer (1999, hereafter SU) and Magorrian & Tremaine (1999, hereafter MT). Both groups took black hole masses from the Magorrian et al. (1998) demographic study, which found a mean ratio of black hole mass to bulge mass of ~ 0.006 . Following the discovery of the $M_\bullet - \sigma$ relation (Ferrarese & Merritt 2000, Gebhardt et al. 2000), the mean value of M_\bullet / M_{bulge} was revised downward, to ~ 0.001 (Merritt & Ferrarese 2001a, Kormendy & Gebhardt 2001). The lower mean value of M_\bullet / M_{bulge} resolved two outstanding discrepancies: the factor ~ 10 difference between black hole masses in quiescent and active galaxies with similar luminosities (Wandel 1999); and the higher apparent density of black holes in nearby galaxies compared with what is needed to explain the integrated light from quasars (Richstone et al. 1998).

Here we examine the consequences of downwardly revised black hole masses for the rate of stellar tidal disruptions in galactic nuclei. Published scaling relations (e.g. Frank & Rees 1976; Cohn & Kulsrud 1978) suggest that stellar consumption rates in galactic nuclei should scale as $\sim M_\bullet^n$, $4/3 \lesssim n \lesssim 9/4$ when the other properties (density, velocity dispersion) of the host galaxy are fixed. Hence one might naively expect the lower values of M_\bullet to imply lower rates of stellar disruption. Instead we find the opposite: in most galaxies, and in particular in the galaxies with steep nuclear density profiles that dominate the overall event rate, decreasing the assumed value of M_\bullet leads to *higher* rates of loss cone feeding. We estimate a total tidal disruption rate among non-dwarf galaxies that is about an order of magnitude higher than in studies based on the Magorrian et al. black hole masses.

This paper is laid out as follows. §2 describes the galaxy sample and §3 reviews the steady-state loss cone theory from which event rates are computed. The theory is applied in §4, with the counter-intuitive result that lower values of M_\bullet imply greater feeding rates in most galaxies. This result is analyzed in more detail in §5, where it is shown to be a generic property of steep power-law nuclei. We derive an accurate, analytical expression for the tidal disruption rate in singular isothermal sphere nuclei. In §6 we present the implications of our results for the overall rate of tidal flaring and show that the predicted rate would be so high in dwarf galaxies that the presence of black holes in these systems could be ruled out by just a few years’ monitoring of a rich galaxy cluster like Virgo. §7 sums up.

2. GALAXY SAMPLE

Our basic sample is the set of 61 elliptical galaxies whose surface brightness profiles were studied by Faber et al. (1997). These authors fit the luminosity data to the parametric model

$$I(\xi) = I_b 2^{\frac{\beta-\Gamma}{\alpha}} \xi^{-\Gamma} (1 + \xi^\alpha)^{-\frac{\beta-\Gamma}{\alpha}}, \quad \xi \equiv R/r_b \quad (1)$$

where r_b is the “break radius,” $I_b = I(r_b)$, and Γ is the logarithmic slope of the surface brightness profile at small radii. (Note that we adopt the “theorist’s convention” in which γ refers to the logarithmic slope of the central *space* density profile.) For 51 of these galaxies, Faber et al. (1997) give values for each

of the five parameters $\mu_b, \alpha, \beta, \Gamma$ and Υ_V ; the latter is the visual mass-to-light ratio assuming $H_0 = 80 \text{ km s}^{-1} \text{ Mpc}^{-1}$ and μ_b is the surface brightness at r_b in visual magnitudes arcsec^{-2} . For these 51 galaxies we computed the mass density profile via Abel's equation:

$$\rho(r) = \Upsilon_V j(r) = -\frac{\Upsilon_V}{\pi} \int_r^\infty \frac{dI}{dR} \frac{dR}{\sqrt{R^2 - r^2}} \quad (2)$$

with $j(r)$ the luminosity density. Below we follow the convention of referring to galaxies with $\Gamma \lesssim 0.2$ as ‘‘core’’ galaxies and those with $\Gamma \gtrsim 0.2$ as ‘‘power-law’’ galaxies.¹ We note that even most core galaxies exhibit an approximately power-law dependence of space density on radius for small r , $\rho \sim r^{-\gamma}$ (Merritt & Fridman 1996, Gebhardt et al. 1996). The weak power-law dependence ρ on r in the core galaxies is not well reproduced by deprojection of the fitting function (1), which is a possible source of systematic error in what follows. Our sample (Table 1) contains 28 power-law galaxies and 23 core galaxies.

The gravitational potential $\psi(r) \equiv -\Phi(r)$ was computed via

$$\psi(r) = \psi_*(r) + \frac{GM_\bullet}{r}, \quad (3a)$$

$$\psi_*(r) = \frac{4\pi G}{r} \int_r^\infty \rho(r') r'^2 dr' + 4\pi G \int_r^\infty \rho(r') r' dr' \quad (3b)$$

$$= \frac{GM(r)}{r} - 4\pi G \int_r^\infty \frac{\Upsilon_V}{\pi} \int_{r'}^\infty \frac{dI(R)}{dR} \frac{dR}{\sqrt{R^2 - r'^2}} r' dr' \quad (3c)$$

$$= \frac{GM(r)}{r} + 2^{2+\frac{\beta-\gamma}{\alpha}} G \Upsilon_V r_b^\beta \int_r^\infty (\Gamma r_b^\alpha + \beta r'^\alpha) r'^{\gamma-1} (r_b^\alpha + r'^\alpha)^{-(1-\frac{\beta-\gamma}{\alpha})} \sqrt{r'^2 - r^2} dr'. \quad (3d)$$

The distribution function f , defined as the number density of stars in phase space, was computed via Eddington's formula:

$$f(\varepsilon) = \frac{1}{\sqrt{8\pi^2 m_*}} \frac{d}{d\varepsilon} \int_0^\varepsilon \frac{d\rho}{d\psi} \frac{d\psi}{\sqrt{\varepsilon - \psi}} \quad (4)$$

with m_* the stellar mass and $\varepsilon \equiv -E$. We follow MT in assuming an isotropic velocity distribution. Galaxies with $\Gamma \lesssim 0.05$ were found to have $f < 0$ when $M_\bullet > 0$; this is a consequence of the fact that an isotropic f can not reproduce a shallow density profile around a point mass. The 10 galaxies with negative f 's are included at the end of Table 1 and not discussed further here.

We define the sphere of influence of the black hole to have radius r_h , where

$$M_*(r_h) = 2M_\bullet \quad (5)$$

and M_* is the mass in stars within r . This definition is equivalent to $r_h = GM_\bullet/\sigma^2$ when $\rho(r) \propto r^{-2}$. We further define $\varepsilon_h \equiv \psi(r_h)$.

Of the 41 galaxies in our sample with non-negative f 's, 18 have black hole masses tabulated in Magorrian et al. (1998). These masses are given in column 11 of Table 1. For the remaining galaxies, we give in column 11 black holes masses computed from

$$M_\bullet = 0.006 M_{bulge} \quad (6)$$

the mean relation between bulge mass and black hole mass found by Magorrian et al. (1998).

A second way to estimate black hole masses is via the $M_\bullet - \sigma$ relation (Ferrarese & Merritt 2000; Gebhardt et al. 2000). We adopt the updated version from the review of Merritt & Ferrarese (2001b):

$$M_\bullet = 1.48 \times 10^8 \mathcal{M}_\odot \left(\frac{\sigma_c}{200 \text{ km s}^{-1}} \right)^{4.65}; \quad (7)$$

the errors in the normalizing coefficient and exponent are $\pm 0.24 \times 10^8 \mathcal{M}_\odot$ and ± 0.48 respectively. Equation (7) was determined from a fit to the small sample of galaxies in which the black hole's sphere of influence is clearly resolved. The parameter σ_c in equation (7) is the velocity dispersion measured in an aperture of size $r_e/8$ centered on the nucleus, with r_e the effective radius (Ferrarese & Merritt 2000). We computed σ_c from published measurements of the central velocity dispersion following the prescription in Ferrarese & Merritt (2000). The $M_\bullet - \sigma$ masses are listed in column 13 of Table 1.

As can be seen in Table 1, and discussed in detail elsewhere (e.g. Ferrarese & Merritt 2000; Merritt & Ferrarese 2001b), the Magorrian et al. masses are systematically high compared with masses computed via the $M_\bullet - \sigma$ relation. It is this discrepancy which motivated the current study; both published studies of stellar disruption rates in galactic nuclei (SU, MT) were based on the Magorrian et al. masses.

3. LOSS CONE THEORY

Stars of mass m_* and radius r_* that come within a distance

$$r_t = (\eta^2 \frac{M_\bullet}{m_*})^{1/3} r_* \quad (8)$$

of the black hole will be tidally disrupted; $\eta \approx 0.844$ for an $n = 3$ polytrope. Following MT, we define the ‘‘consumption rate’’ \dot{N} as the rate at which stars come within r_t , even if r_t falls below the Schwarzschild radius $2GM_\bullet/c^2$; the latter occurs when $M_\bullet \gtrsim 10^8 \mathcal{M}_\odot$. (The largest consumption rates occur in small dense galaxies for which $r_t > r_s$.) In a spherical galaxy, stellar orbits lie within the consumption loss cone if their energy ε and angular momentum per unit mass J satisfy

$$J^2 \leq J_c^2(\varepsilon) \equiv 2r_t^2 [\psi(r_t) - \varepsilon] \simeq 2GM_\bullet r_t. \quad (9)$$

We adopt the Cohn-Kulsrud (1978; hereafter CK) formalism for computing the flux of stars into the loss cone. Let $\mathcal{F}(\varepsilon)$ be the number of stars per unit time and unit energy that are deflected into the loss cone via gravitational encounters with other stars. Define $\langle (\Delta R)^2 \rangle$ to be the diffusion coefficient in $R \equiv J^2/J_c^2(\varepsilon)$, with $J_c(\varepsilon)$ the angular momentum of a circular orbit of energy ε . Then (CK)

$$\mathcal{F}(\varepsilon) d\varepsilon = 4\pi^2 J_c^2 \left\{ \oint \frac{dr}{v_r} \lim_{R \rightarrow 0} \frac{\langle (\Delta R)^2 \rangle}{2R} \right\} \frac{f}{\ln R_0^{-1}} d\varepsilon \quad (10)$$

and the total consumption rate is given by

$$\dot{N} = \int \mathcal{F}(\varepsilon) d\varepsilon. \quad (11)$$

In equation (10), $R_0(\varepsilon)$ is the value of R at which f falls to zero due to removal of stars that scatter into the loss cone. R_0 is not

¹In fact we retain the Faber et al. (1997) classifications in Table 1, which are slightly different.

equal to its geometrical value, $R_{lc} = J_{lc}^2/J_c(\varepsilon)^2$, because scattering of stars *onto* loss cone orbits permits f to be nonzero even for $J < J_{lc}$. CK find that $R_0(\varepsilon)$ can be well approximated by

$$R_0(\varepsilon) = R_{lc}(\varepsilon) \times \begin{cases} \exp(-q), & q(\varepsilon) > 1 \\ \exp(-0.186q - 0.824\sqrt{q}), & q(\varepsilon) < 1 \end{cases}, \quad (12)$$

with

$$q(\varepsilon) \equiv \frac{1}{R_{lc}(\varepsilon)} \oint \frac{dr}{v_r} \lim_{R \rightarrow 0} \frac{\langle (\Delta R)^2 \rangle}{2R} = \frac{P(\varepsilon)\bar{\mu}(\varepsilon)}{R_{lc}(\varepsilon)}, \quad (13)$$

$P(\varepsilon)$ is the period of a radial orbit with energy ε and $\bar{\mu}$ is the orbit-averaged diffusion coefficient. The function $q(\varepsilon)$ can be interpreted as the ratio of the orbital period to the time scale for diffusional refilling of the loss cone; $q \gg 1$ defines the ‘‘pin-hole’’ or ‘‘full loss cone’’ regime in which encounters replenish loss cone orbits much more rapidly than they are depleted. MT give expressions for the local angular-momentum diffusion coefficient:

$$\lim_{R \rightarrow 0} \frac{\langle (\Delta R)^2 \rangle}{2R} = \frac{32\pi^2 r^2 G^2 m_*^2 \ln \Lambda}{3J_c^2} (3I_{1/2} - I_{3/2} + 2I_0), \quad (14a)$$

$$I_0 \equiv \int_0^\varepsilon f(\varepsilon') d\varepsilon', \quad (14b)$$

$$I_{\frac{1}{2}} \equiv [2(\psi(r) - \varepsilon)]^{-\frac{1}{2}} \int_\varepsilon^{\psi(r)} [2(\psi(r) - \varepsilon')]^{3/2} f(\varepsilon') d\varepsilon' \quad (14c)$$

from which the orbit-averaged quantities $\bar{\mu}(\varepsilon)$ and $q(\varepsilon)$ can be computed.

In the Fokker-Planck approximation under which equation (10) was derived, the flux of stars into the loss cone at each energy is determined by gradients in f with respect to R at $R \approx R_{lc}$. CK, who modelled globular clusters, derived expressions for these gradients by assuming that the distribution of stars near the loss cone had evolved to a steady state in which the encounter-driven supply of stars into the loss cone was balanced by consumption. Relaxation times in galactic nuclei are usually in excess of a Hubble time, particularly in the core galaxies (Faber et al. 1997), and it is not clear that the distribution of stars near the loss cone will have had time to reach a steady state in all of our galaxies (Milosavljevic & Merritt 2003). We will return to this question in a subsequent paper; for now, we follow MT in assuming that the CK loss cone boundary solution applies to galactic nuclei.

4. DEPENDENCE OF THE CONSUMPTION RATE ON M_\bullet IN THE GALAXY SAMPLE

Figures 1 and 2 show how the energy dependence of various quantities changes with the assumed value of M_\bullet in two galaxies: NGC 4551, a power-law galaxy ($\Gamma = 0.8$); and NGC 4168, a core galaxy ($\Gamma = 0.14$). The value of Υ_V , and hence the mass density of the stars, was fixed as M_\bullet was varied. We adopted $m_* = M_\odot$ throughout. In the power-law galaxy, as M_\bullet is decreased, the flux of stars into the loss cone increases at $\varepsilon \gtrsim \varepsilon_h$ and decreases at $\varepsilon \lesssim \varepsilon_h$; since most of the flux comes from near the black hole, $\varepsilon \gtrsim \varepsilon_h$, the total consumption rate increases with decreasing M_\bullet . In the core galaxy, the dependence of $\mathcal{F}(\varepsilon)$ on M_\bullet is more complex: $\mathcal{F}(\varepsilon \approx \varepsilon_h)$ first increases, then decreases, with decreasing M_\bullet . The consequences of these trends can be seen in Figure 3, which plots integrated consumption rates \dot{N}

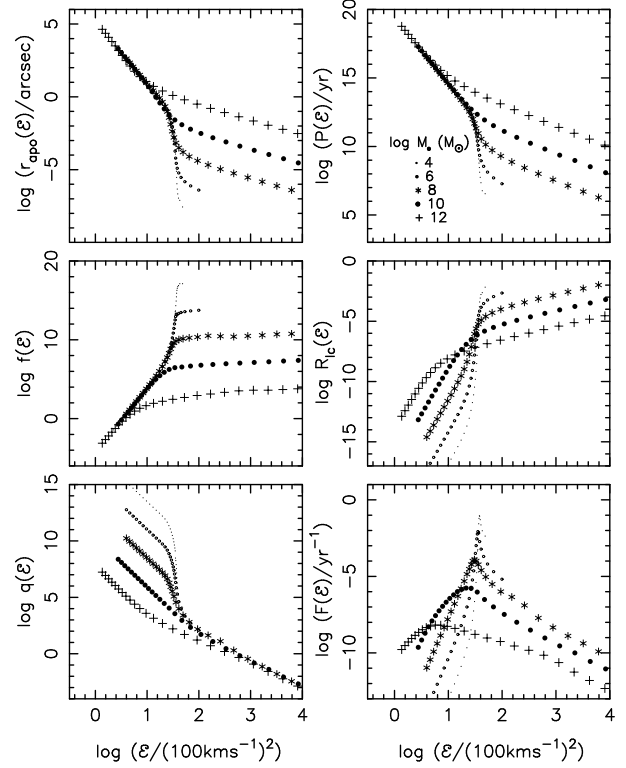


FIG. 1.— Dependence on M_\bullet of various quantities associated with stellar consumption in the power-law galaxy NGC 4551. Stars are assumed to have solar mass and radius. Left column: r_{apo} (apocenter radius of radial orbit); f (phase space number density); q (quantity that distinguishes between diffusion and full-loss-cone regimes). Right column: P (period of radial orbit); R_{lc} (geometric size of loss cone in terms of $R \equiv J^2/J_c^2$); \mathcal{F} (flux into loss cone). As M_\bullet is reduced, more and more of the galaxy falls within the full-loss-cone regime ($q \gg 1$) and the total flux of stars into the loss cone rises.

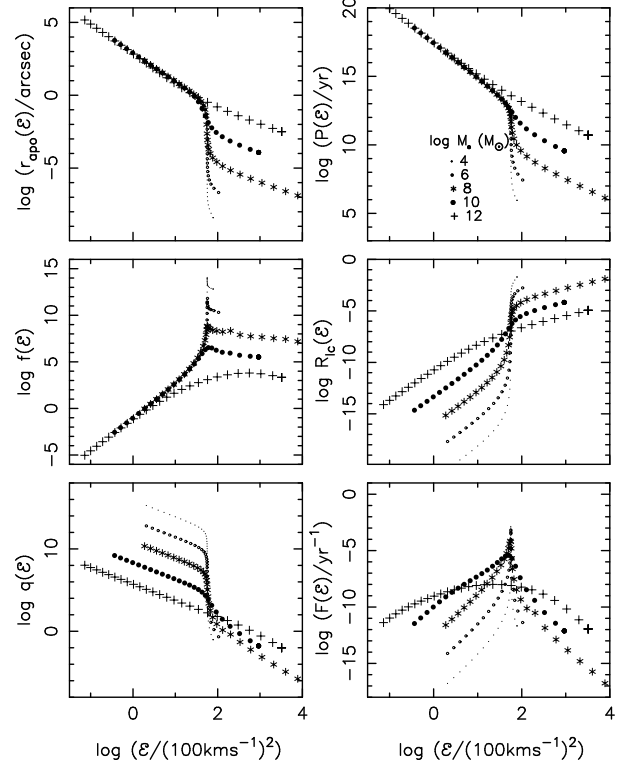


FIG. 2.— Like Figure 1, but for the core galaxy NGC 4168. By comparison with NGC 4551, less of the galaxy lies in the full-loss-cone regime and the total consumption rate is lower.

as a function of M_\bullet for every galaxy in our sample. The power-law galaxies exhibit monotonic or nearly monotonic trends of increasing \dot{N} with decreasing M_\bullet ; the dependence is roughly $\dot{N} \propto M_\bullet^{-1}$. In the case of the core galaxies, \dot{N} generally increases with M_\bullet up to a maximum value, then decreases as M_\bullet is increased further. This behavior is explained in the next section.

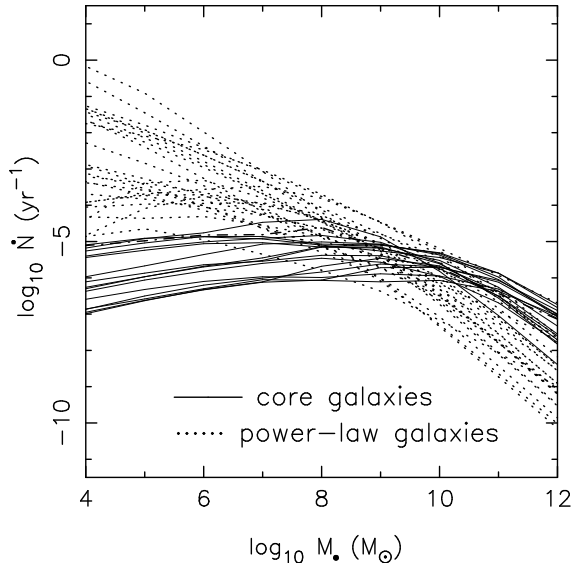


FIG. 3.— Dependence of consumption rate on assumed black hole mass for the galaxies in Table 1.

Our primary concern is how consumption rates would change if the black hole masses used by earlier authors were replaced with the presumably more accurate masses derived from the $M_\bullet - \sigma$ relation. Figure 4 makes this comparison. In almost every galaxy in our sample, the inferred \dot{N} is greater when the $M_\bullet - \sigma$ black hole mass is used. The changes are greatest in the power-law galaxies, since $\dot{N} \sim M_\bullet^{-1}$ in these galaxies. In the core galaxies, although M_\bullet is sometimes increased by as much as 10^2 , the changes in \dot{N} are usually modest because of the nearly flat dependence of \dot{N} on M_\bullet in these galaxies (Figure 3).

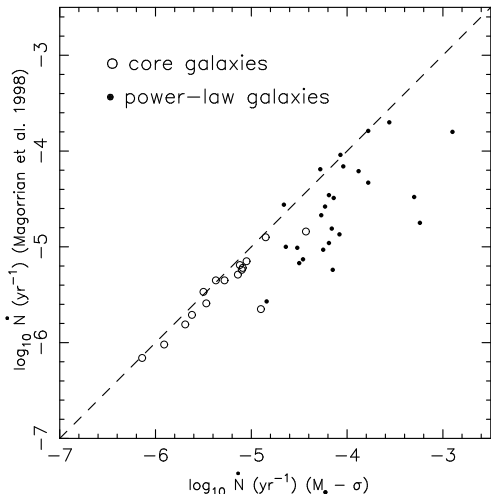


FIG. 4.— Comparison of consumption rates computed using the two values of M_\bullet in Table 1. Abscissa: M_\bullet computed from the $M_\bullet - \sigma$ relation, equation (7). Ordinate: M_\bullet from Magorrian et al. (1998).

Figure 5 shows the dependence of \dot{N} on galaxy luminosity and M_\bullet in our sample; black hole masses were taken from the $M_\bullet - \sigma$ relation. The dependence of flaring rate on M_\bullet is fairly tight, with a mean slope of $\dot{N} \sim M_\bullet^{-0.8}$.

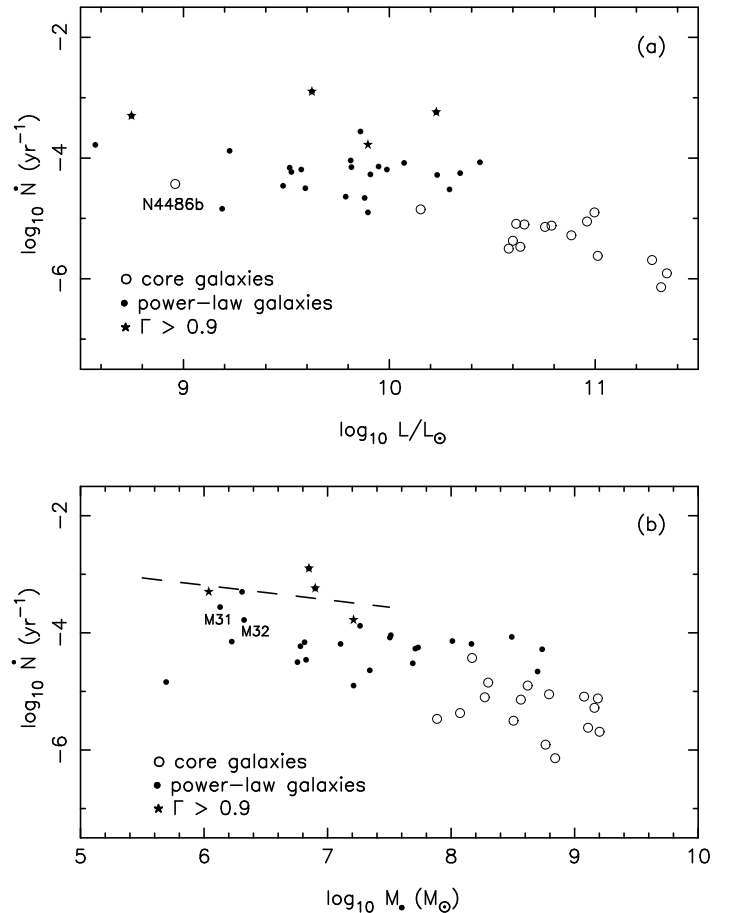


FIG. 5.— Consumption rate as a function of galaxy luminosity (a) and black hole mass (b). The dashed line in (b) is the relation defined by the singular isothermal sphere, eq. (29); it is a good fit to the galaxies plotted with stars, which have steep central density profiles, $\rho \sim r^{-2}$.

Figure 6 shows how \dot{N} and three critical radii associated with the black hole vary with M_\bullet in NGC 4551 and NGC 4168. The tidal radius r_t and the radius of influence r_h were defined above. The third radius, r_{crit} , is defined as:

$$\psi(r_{crit}) = \varepsilon_{crit}, \quad q(\varepsilon_{crit}) = 1. \quad (15)$$

r_{crit} is roughly the radius of transition between the “diffusive” ($q < 1$) and “full-loss-cone” ($q > 1$) regimes, and most of the flux into the loss cone comes from radii $r \lesssim r_{crit}$. We note that $r_{crit} \lesssim r_h$ over the relevant range in M_\bullet for both galaxies, and that both r_t and r_{crit} are less than r_b . These same inequalities were found to hold for most of the galaxies in our sample, which motivated the simplified treatment in the following section.

5. DEPENDENCE OF CONSUMPTION RATE ON M_\bullet IN POWER-LAW NUCLEI

We noted above the curious behavior of \dot{N} as M_\bullet is varied in a galaxy with otherwise fixed properties: \dot{N} generally increases as M_\bullet is reduced. Here we show how the dependence of \dot{N} on

M_\bullet can be understood. We derive the exact consumption rate in a $\rho \propto r^{-2}$ galaxy, which is a good model for the faintest galaxies in our sample, then derive approximate scaling relations for the dependence of \dot{N} on M_\bullet in nuclei with shallower power-law indices.

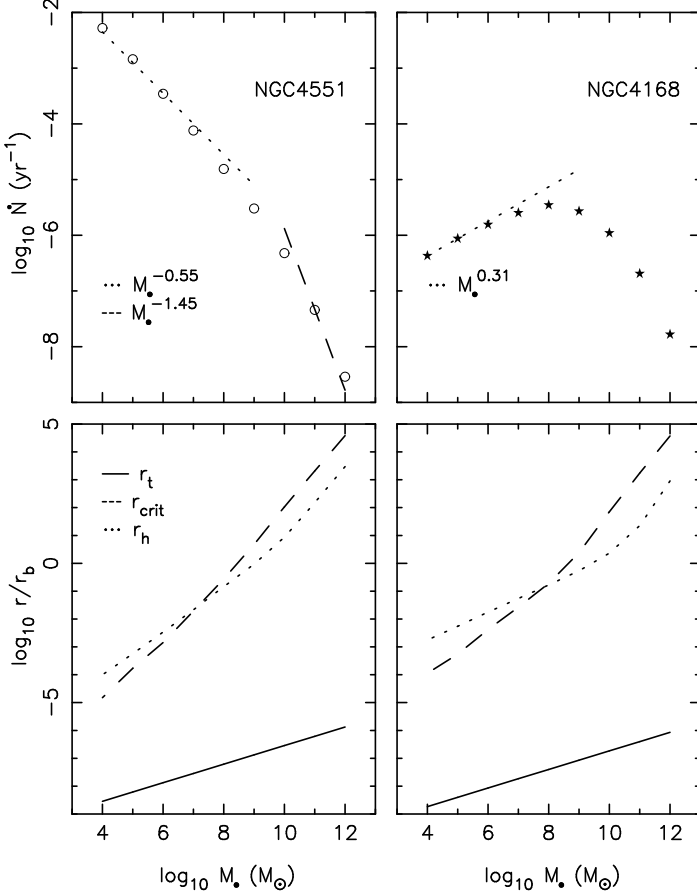


FIG. 6.— Top panels: dependence of consumption rate on M_\bullet in NGC 4551 (power-law galaxy) and NGC 4168 (core galaxy). Dashed lines are the approximate M_\bullet -dependences derived in §5.2. Bottom panels: M_\bullet -dependence of three characteristic radii: r_t , the tidal disruption radius; r_{crit} , the radius dividing the diffusive- and full-loss-cone regimes; and r_h , the black hole's radius of influence. r_b is the break radius of the luminosity profile.

5.1. The Singular Isothermal Sphere

Faint galaxies like M32 have the greatest consumption rates. These galaxies also have steep power-law nuclear density profiles, $\rho \sim r^{-\gamma}$, $\gamma \approx 2$. Since r_{crit} is generally less than r_b in our galaxies (cf. Figure 6), we can approximate the stellar density profile as a single power law when computing the flux. Here we consider the singular isothermal sphere (SIS), $\gamma = 2$. The SIS density profile and potential are

$$\rho(r) = \frac{\sigma^2}{2\pi G r^2}, \quad \psi_*(r) = -2\sigma^2 \ln\left(\frac{r}{r_h}\right), \quad r_h \equiv \frac{GM_\bullet}{\sigma^2} \quad (16)$$

where σ is the 1D stellar velocity dispersion, independent of radius for $r \gtrsim r_h$. The potential due to the stars has been normalized to zero at $r = r_h$, and $\psi(r) = \psi_*(r) + GM_\bullet/r$. The isotropic distribution function describing the stars is

$$f(\varepsilon) = \frac{1}{\sqrt{8\pi^2 m_*}} \frac{d}{d\varepsilon} \int_0^\varepsilon \frac{d\rho}{d\psi} \frac{d\psi}{\sqrt{\varepsilon - \psi}} \quad (17a)$$

$$= \frac{1}{r_h^3 \sigma^3} \left(\frac{M_\bullet}{m_*}\right) g^*(\varepsilon^*), \quad (17b)$$

$$g^*(\varepsilon^*) = \frac{\sqrt{2}}{4\pi^3} \int_{-\infty}^{\varepsilon^*} \frac{L^2(u)[2+L(u)]}{[1+L(u)]^3} \frac{d\psi^*}{\sqrt{\varepsilon^* - \psi^*}},$$

$$u(\psi^*) \equiv \frac{1}{2} e^{\psi^*/2}. \quad (17c)$$

$L(u)$ is the Lambert function (also called the W function) defined implicitly via $u = Le^L$. The superscript “*” denotes dimensionless quantities and the units of mass and velocity are

$$[M] = M_\bullet, \quad [V] = \sigma \quad (18)$$

with $G = 1$. The dimensionless function $q(\varepsilon^*)$ that characterizes the deflection amplitude per orbital period is

$$q(\varepsilon^*) = \frac{32\pi^2}{3\sqrt{2}} \ln \Lambda \left(\frac{m_*}{M_\bullet}\right) \frac{h^*(\varepsilon^*)}{\psi^*(r_t) - \varepsilon^*} \left(\frac{r_t}{r_h}\right)^{-2} \quad (19)$$

and the loss cone flux is

$$\mathcal{F}^*(\varepsilon^*) = \frac{256\pi^4}{3\sqrt{2}} \frac{\ln \Lambda}{\ln R_0^{-1}} g^*(\varepsilon^*) h^*(\varepsilon^*), \quad (20)$$

where

$$h^*(\varepsilon^*) = h_1^*(\varepsilon^*) + h_2^*(\varepsilon^*) + h_3^*(\varepsilon^*), \quad (21a)$$

$$h_1^*(\varepsilon^*) = 2 \left[\int_{-\infty}^{\varepsilon^*} g^*(\varepsilon'^*) d\varepsilon'^* \right] \left[\int_0^{r^*(\varepsilon'^*)} \frac{dr^* r^{*2}}{\sqrt{\psi^*(r^*) - \varepsilon'^*}} \right], \quad (21b)$$

$$h_2^*(\varepsilon^*) = 3 \int_0^{r^*(\varepsilon^*)} \frac{dr^* r^{*2}}{\psi^*(r^*) - \varepsilon^*} \int_{\varepsilon^*}^{\psi^*(r^*)} d\varepsilon'^* \sqrt{\psi^*(r^*) - \varepsilon'^*} g^*(\varepsilon'^*), \quad (21c)$$

$$h_3^*(\varepsilon^*) = - \int_0^{r^*(\varepsilon^*)} \frac{dr^* r^{*2}}{[\psi^*(r^*) - \varepsilon^*]^2} \int_{\varepsilon^*}^{\psi^*(r^*)} d\varepsilon'^* [\psi^*(r^*) - \varepsilon'^*]^{3/2} g^*(\varepsilon'^*) \quad (21d)$$

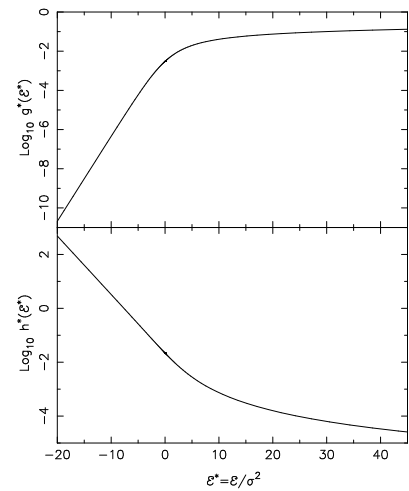


FIG. 7.— Dimensionless functions $g^*(\varepsilon^*)$, $h^*(\varepsilon^*)$ that characterize the phase-space density and angular momentum diffusion coefficient (equations 17c, 21) in a singular isothermal sphere galaxy.

Note that the functions $g^*(\varepsilon^*)$ and $h^*(\varepsilon^*)$ are determined uniquely in these dimensionless units. These functions are plotted in Figure 7.

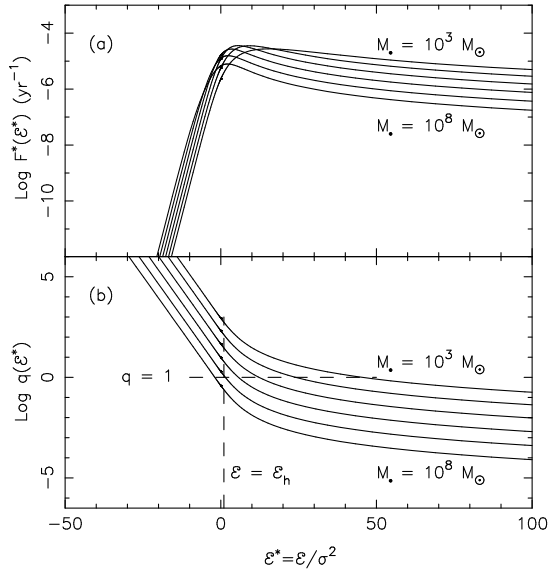


FIG. 8.— Dimensionless loss-cone flux \mathcal{F}^* (equation 20) and q (equation 19) as functions of energy in a singular isothermal sphere galaxy, for various values of M_\bullet . The M_\bullet - σ relation (equation 7) was used to relate σ to M_\bullet .

The function $R_0(\varepsilon)$ that defines the edge of the loss cone is given by equation (12), with

$$R_{lc}(\varepsilon) = 2 \left(\frac{r_t}{r_h} \right)^2 \frac{\psi^*(r_t^*) - \varepsilon^*}{(2 + r_c^{*-1}) r_c^{*2}}, \quad r_c^*(\varepsilon^*) = 1/4L \left[e^{-(1-\varepsilon^*)/2} / 4 \right]; \quad (22)$$

$r_c(\varepsilon)$ is the radius of a circular orbit of energy ε .

If we set $\Lambda = 0.4M_\bullet/m_*$ (Spitzer & Hart 1971), the dimensionless flux $\mathcal{F}^*(\varepsilon^*)$ is determined by the two parameters

$$\left(\frac{M_\bullet}{m_*}, \frac{r_h}{r_t} \right). \quad (23)$$

Adopting equation (8) for r_t , we can write the second of these two parameters as

$$\frac{r_h}{r_t} = \frac{2\Theta}{\eta^{2/3}} \left(\frac{M_\bullet}{m_*} \right)^{2/3} \quad (24a)$$

$$= 21.5 \left(\frac{M_\bullet}{m_*} \right)^{2/3} \left(\frac{\sigma}{100 \text{ km s}^{-1}} \right)^{-2} \left(\frac{m_*}{M_\odot} \right) \left(\frac{r_*}{\mathcal{R}_\odot} \right)^{-1} \quad (24b)$$

with $\Theta \equiv Gm_*/2\sigma^2 r_*$ the Safronov number; η has been set to 0.844. Given values for m_* and r_* , the two parameters that specify $\mathcal{F}(E)$ are then M_\bullet and σ .

Figure 8a shows $\mathcal{F}^*(\varepsilon^*)$ for various values of M_\bullet ; σ was computed from M_\bullet via the M_\bullet - σ relation (7). The flux exhibits a mild maximum at $\varepsilon \approx \varepsilon_h$ and falls off slowly toward large (bound) energies. The function $q(\varepsilon^*)$ is shown in Figure 8b. As M_\bullet is reduced, more and more of the nucleus lies within the full-loss-cone regime, $q \gg 1$.

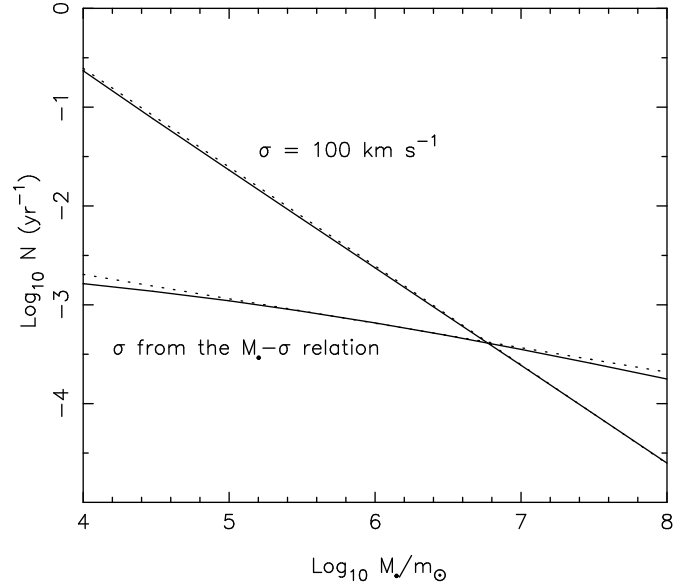


FIG. 9.— Consumption rate as a function of M_\bullet in singular isothermal sphere nuclei, under two assumptions about $\sigma(M_\bullet)$. Dashed lines: equation (29).

Figure 9 shows the consumption rate $\dot{N} = \int \mathcal{F}(E) dE$ as a function of M_\bullet under two assumptions about the relation of σ to M_\bullet : $\sigma = 100 \text{ km s}^{-1}$; or σ determined from the M_\bullet - σ relation (7). For fixed σ , Figure 9 shows that $\dot{N} \sim M_\bullet^{-1}$, while allowing σ to vary with M_\bullet implies a weaker (but still inverse) dependence of \dot{N} on M_\bullet .

The scaling of the consumption rate with M_\bullet and σ can be derived in a straightforward way. Figure 8 shows that over a wide range of M_\bullet values, most of the flux comes from $\varepsilon \gtrsim \varepsilon_h$. In this energy interval, $\psi^*(r^*) \approx GM_\bullet/r^*$ and

$$g^*(\varepsilon^*) \approx \frac{1}{\sqrt{2}\pi^3} \varepsilon^{1/2}, \quad h^*(\varepsilon^*) \approx \frac{5\sqrt{2}}{24\pi^2} \varepsilon^{*-2}; \quad (25)$$

the latter expression makes use of the fact that $h^* \approx h_1^*$, i.e. most of the flux comes from scattering by stars with energies greater than that of the test star. Thus

$$q(\varepsilon^*) \approx \frac{20}{9} \ln \Lambda \left(\frac{m_*}{M_\bullet} \right) \left(\frac{r_h}{r_t} \right) \varepsilon^{*-2} \quad (26)$$

and $R_{lc} \approx 4(r_t/r_h)\varepsilon^*$. The dimensionless flux is

$$\mathcal{F}^*(\varepsilon^*) \approx \frac{160 \ln \Lambda}{9\sqrt{2}\pi} \varepsilon^{*1/2} \left[A + \varepsilon^{*2} \ln \left(\frac{B}{\varepsilon^*} \right) \right]^{-1}, \quad (27a)$$

$$A \equiv \frac{20}{9} \ln \Lambda \left(\frac{m_*}{M_\bullet} \right) \left(\frac{r_h}{r_t} \right), \quad (27b)$$

$$B \equiv \frac{r_h}{4r_t}. \quad (27c)$$

Ignoring the weak E -dependence of the logarithmic term and taking r_h/r_t from equation (24b), we find

$$\dot{N} = \int \mathcal{F}(E) dE \propto A^{-1/4} \propto \sigma^{7/2} M_\bullet^{-11/12}. \quad (28)$$

After some experimentation, we found that the following, slightly different scaling:

$$\dot{N} \approx 7.1 \times 10^{-4} \text{yr}^{-1} \left(\frac{\sigma}{70 \text{ km s}^{-1}} \right)^{7/2} \left(\frac{M_\bullet}{10^6 M_\odot} \right)^{-1}, \quad (29)$$

provides a better fit to the exact, numerically-computed feeding rates over the relevant range in M_\bullet (Figure 9). The normalization constant in equation (29) was chosen to reproduce \dot{N} exactly for $\sigma = 70 \text{ km s}^{-1}$, $M_\bullet = 10^6 M_\odot$. The consumption rate in equation (29) was derived assuming stars of solar mass and radius and scales as $m_\star^{-1/3} r_\star^{1/4}$.

5.2. Shallower Power-Law Profiles

The bright galaxies in our sample have nuclear density profiles with shallower power-law indices, $\rho \sim r^{-\gamma}$, $\gamma \lesssim 2$. We calculate the dependence of \dot{N} on M_\bullet in these galaxies using a more approximate approach.

The flux of stars into the loss cone, equation (10), can be written

$$\mathcal{F}(E) = \frac{\mathcal{F}_{\max}(E)}{\ln R_0^{-1}}, \quad (30a)$$

$$\mathcal{F}_{\max}(E) \equiv 4\pi^2 P(E) J_c^2(E) \bar{\mu}(E) f(E) \quad (30b)$$

$$\approx \bar{\mu}(E) N(E) \quad (30c)$$

with $N(E)$ the number of stars per unit energy interval; equation (30c) assumes that $P(E, J) \approx P(E)$. Now $\mu \equiv 2r^2 \langle \Delta v_r^2 \rangle / J_c^2$, a function both of r and E , and its orbit-averaged value $\bar{\mu}$ can be interpreted as the time-averaged inverse of the relaxation time T_R for orbits of energy E . Hence

$$\mathcal{F}(E) \approx \frac{N(E)}{T_R(E)} \frac{1}{\ln R_0^{-1}(E)}. \quad (31)$$

Above some energy E_{crit} , $R_0 \approx R_{lc} e^{-q}$ falls off rapidly with increasing E , while for $E \lesssim E_{\text{crit}}$, $R_0 \approx R_{lc}$ and $\ln R_0^{-1}$ is a slowly-varying function of order unity. Hence

$$\dot{N} \approx \int_{-\infty}^{E_{\text{crit}}} \frac{N(E)}{T_R(E)} dE \quad (32a)$$

$$\approx \frac{N(r < r_{\text{crit}})}{T_R(r_{\text{crit}})} \quad (32b)$$

where $\Phi(r_{\text{crit}}) \approx E_{\text{crit}}$. These expressions correspond physically to the fact that the time to scatter into the loss cone is comparable to T_R for all $E \lesssim E_{\text{crit}}$. Frank & Rees (1977, hereafter FR) used an equation similar to (32b) to estimate feeding rates in nuclei with constant-density cores. We repeat their analysis here, for black holes in nuclei with arbitrary density slopes:

$$\rho(r) = \rho_0 \left(\frac{r}{r_0} \right)^{-\gamma}. \quad (33)$$

For T_R we take the Spitzer & Harm (1958) reference time:

$$T_R(r) = \frac{\sqrt{2}\sigma^3(r)}{\pi G^2 m_\star \rho(r) \ln \Lambda}. \quad (34)$$

Since $r_{\text{crit}} \lesssim r_h$ (Figure 6), we can write $\sigma^2(r) \approx GM_\bullet/r$ and

$$\dot{N} \approx \frac{N(r < r_{\text{crit}})}{T_R(r_{\text{crit}})} \propto (3-\gamma)^{-1} \ln \Lambda G^{1/2} \rho_0^2 r_0^{9/2} M_\bullet^{-3/2} \left(\frac{r_{\text{crit}}}{r_0} \right)^{9/2-2\gamma}. \quad (35)$$

Following FR, we define r_{crit} to be the radius above which encounters can scatter stars into or out of the loss cone in a single orbital period; at this radius, $q \approx 1$. At $r = r_{\text{crit}}$, the angular size of the loss cone, θ_{lc} , is comparable to the angle θ_d by which a star is deflected in a single period; taking account of gravitational focussing, $\theta_{lc} \approx \sqrt{r_t/r}$. We adopt equation (8) for r_t and write $\theta_d^2 \approx P/T_r \approx \sqrt{r^3/GM_\bullet}/T_r$; the square root dependence of θ_d on P reflects the fact that entry into the loss cone is a diffusive process. Setting $\theta_{lc} = \theta_d$ then gives

$$\left(\frac{r_{\text{crit}}}{r_0} \right)^{4-\gamma} = \text{Constant} \times (\ln \Lambda)^{-1} m_\star^{-1} \rho_0^{-1} r_0^{-4} M_\bullet^{7/3} \quad (36)$$

and for fixed (ρ_0, r_0) ,

$$\dot{N} \propto M_\bullet^\delta, \quad \delta = \frac{27-19\gamma}{6(4-\gamma)}. \quad (37)$$

For the SIS, $\gamma = 2$ and we recover $\delta = -11/12$ (equation 28).

For $\gamma < 27/19 = 1.42$, equation (37) gives $\delta > 0$ and \dot{N} increases with increasing M_\bullet ; for instance, setting $\gamma = 0$ gives the constant-density core and $\dot{N} \propto M_\bullet^{1.1}$. This explains why the tidal destruction rates in the ‘‘core’’ galaxies generally increase with increasing M_\bullet . As M_\bullet is increased still further in these galaxies, \dot{N} drops, since $r_h > r_b$ and the effective power-law index becomes steeper. Figure 6 shows fits of equation (28) to $\dot{N}(M_\bullet)$ for two galaxies.

6. IMPLICATIONS FOR THE DETECTION OF FLARES

Black hole mass is observed to correlate tightly with bulge velocity dispersion (Ferrarese & Merritt 2000, Gebhardt et al. 2000), and with bulge mass (Merritt & Ferrarese 2001a) and luminosity (McLure & Dunlop 2002, Erwin, Graham & Caon 2002). Hence we can convert our scaling relation (29) into a net scaling of \dot{N} on L . First combining the $M_\bullet - \sigma$ relation (7) with equation (29):

$$\dot{N} \approx 4.2 \times 10^{-4} \text{yr}^{-1} \left(\frac{\sigma}{100 \text{ km s}^{-1}} \right)^{-1.15} \quad (38a)$$

$$\approx 6.5 \times 10^{-4} \text{yr}^{-1} \left(\frac{M_\bullet}{10^6 M_\odot} \right)^{-0.25}. \quad (38b)$$

Merritt & Ferrarese (2001a) find that $\log_{10} M_\bullet / M_{\text{bulge}}$ is distributed as a Gaussian with mean -2.91 and dispersion 0.45 ; the latter is consistent with being due entirely to measurement errors in M_\bullet . Magorrian et al. (1998) find a mean mass-to-light ratio for their galaxy sample of $\Upsilon_V \approx 4.9 h (L/10^{10} h^{-2} \mathcal{L}_\odot)^{0.18} \Upsilon_\odot$ ($h \equiv H_0/80 \text{ km s}^{-1} \text{ Mpc}^{-1}$). Combining these relations with equation (38b) gives

$$\dot{N} \approx 2.2 \times 10^{-4} \text{yr}^{-1} h^{-0.25} \left(\frac{L}{10^{10} h^{-2} \mathcal{L}_\odot} \right)^{-0.295}. \quad (39)$$

MT derived a similar relation (their ‘‘toy model’’, eq. 58) for consumption in a power-law nucleus. Correcting for different assumed Hubble constants, their relation is

$$\dot{N} \approx 2.6 \times 10^{-5} \text{yr}^{-1} h^{2/3} \left(\frac{L}{10^{10} h^{-2} \mathcal{L}_\odot} \right)^{-0.22}; \quad (40)$$

the different scaling with h results from their use of an effective radius-luminosity relation in place of the $M_\bullet - \sigma$ relation. Our predicted event rate is a factor $\sim 7(12)$ greater than theirs at $L = 10^{10}(10^8)\mathcal{L}_\odot$; these differences result primarily from the larger value (0.006 vs. 0.001) assumed by MT for (M_\bullet/M_{bulge}) , and secondarily from our steeper dependence of \dot{N} on L .

MT derived a total flaring rate for early type galaxies and bulges by combining equation (40) with the Ferguson & Sandage (1991) E + S0 luminosity function and assuming an equal contribution from black holes in bulges. They found a rate per unit volume of $6.6 \times 10^{-7} \text{ yr}^{-1} \text{ Mpc}^{-3}$ ($H_0 = 80$). Comparing equations (40) and (39), we conclude that the downward revision in black hole masses implies roughly an order of magnitude increase in the total event rate, to $\sim 10^{-5} \text{ yr}^{-1} \text{ Mpc}^{-3}$.

The faintest systems in which there is solid kinematical evidence for nuclear black holes are M32 and the bulge of the Milky Way ($L \approx 10^9 \mathcal{L}_\odot, M_\bullet \approx 10^{6.5} \mathcal{M}_\odot$). However there is compelling circumstantial evidence for supermassive black holes in fainter systems (e.g. Filippenko & Ho 2003) and less compelling evidence for intermediate mass black holes (IMBHs) in starburst galaxies and star clusters (van der Marel 2003 and references therein). Here we consider the consequences for the overall tidal flaring rate if nuclear black holes exist in galaxies fainter than M32. The galaxies in question are the dwarf ellipticals, spheroidal systems fainter than $M_V \approx -19$ (Ferguson & Binggeli 1994). In spite of their distinct name, dE galaxies have properties that are a smooth continuation to lower luminosities of the properties of bright ellipticals (Jerjen & Binggeli 1997, Graham & Guzman 2003). The dEs are the most numerous type of galaxy in the universe; in rich galaxy clusters their numbers appear to diverge at low luminosities as $N(L) \sim L^{-1}$ (Ferguson & Sandage 1991). If dE galaxies contain nuclear black holes, they would dominate the total tidal flaring rate due both to their numbers and to their high individual event rates.

Rather than assume that every dE contains a nuclear black hole, we make the more conservative assumption that only the nucleated dEs (dEn's) contain black holes. Most of the dEn's are too distant for their central luminosity profiles to be resolved (e.g. Stiavelli et al. 2001); one exception from the Local Group is NGC 205, in which the deprojected density is observed to increase as $\sim r^{-2}$ inward of $\sim 1 \text{ pc}$ (L. Ferrarese, private communication). This is similar to what is seen in the other, nucleated spheroidal systems in the Local Group with comparable luminosities, namely M32 and the bulges of M31 and M33 (Lauer et al. 1998) and the bulge of the Milky Way (Genzel et al. 2003). We assume that all dEn's have nuclei with a similar structure and that dEn's contain nuclear black holes with the same ratio of black hole mass to total luminosity that is characteristic of brighter galaxies. We can then apply our scaling relations, equations (38a,b,39), to dEn galaxies. We note in passing that the luminosity profiles of the dEn's – a steep nucleus superposed on a shallower background profile – is just what is predicted by “adiabatic growth” models for black holes (Peebles 1972, Young 1980), although there are other possible explanations for the origin of the nuclei (e.g. Freeman 1993).

Van den Bergh (1986) plots the fraction of dEs that are nucleated in a sample of galaxy clusters observed by Binggeli, Sandage & Tammann (1985). He finds a roughly linear relation between the nucleated fraction F_n and absolute magnitude:

$$F_n \approx -0.2(M_V + 13), \quad -18 \lesssim M_V \lesssim -13. \quad (41)$$

The nucleated fraction is unity in dEs brighter than $M_V \approx -18$

and negligible in galaxies fainter than $M_V \approx -13$. Trentham & Tully (2002) derive luminosity functions for the dwarf galaxy populations at the centers of six galaxy clusters including the Virgo cluster. They fit their data to a Schechter function,

$$N(M_R)dM_R = N_d \left(\frac{L}{L_d} \right)^{\alpha_d+1} e^{-L/L_d} dM_R \quad (42)$$

with M_R the R -band absolute magnitude. The normalization factor N_d has units of Mpc^{-2} and gives the surface density of dE galaxies at a distance of 200 kpc from the cluster center. Trentham & Tully find faint-end slopes of $-1.5 \lesssim \alpha_d \lesssim -1$, consistent with earlier determinations (e.g. Sandage, Binggeli & Tamman 1985).

Table 2 gives the tidal flaring rate implied by equations (39), (41) and (42) for the centers of the six clusters analyzed by Trentham & Tully (2002). We give also an event rate for the center of the Coma cluster based on the Secker & Harris (1996) dE luminosity function. The highest event rates, $\sim 0.1 \text{ yr}^{-1} \text{ Mpc}^{-2}$, are predicted for the centers of the Coma and Virgo clusters.

These predicted event rates could be substantially increased by including the contribution from the bulges of late-type spirals, assuming the latter also contain IMBHs. Bulge luminosity profiles are similar to those of dE galaxies (Möllenhoff & Heidt 2001, Balcells et al. 2003) and often exhibit distinct nuclei (Carollo et al. 2002). Balcells, Dominguez-Palmero & Graham (2001) present resolved nuclear density profiles in a sample of spiral bulges observed with HST; the nuclei are well fit by power laws with $1.5 \lesssim \gamma \lesssim 2.5$, similar to what is seen in the nuclei of the Local Group dwarves.

The event rate due to dEn galaxies in the Virgo cluster as a whole can be computed using the determination by Ferguson & Sandage (1989) of the spatial distribution of the dEn's. They find a surface density $\Sigma(R) \approx \Sigma_0 e^{-R/R_0}$, $R_0 \approx 0.48 \text{ Mpc}$, more centrally concentrated than the distribution of non-nucleated dwarves. Using the central density normalization of Trentham & Tully (2002), we find a total rate of tidal flaring due to dwarf galaxies in Virgo of $\sim 0.16 \text{ yr}^{-1}$. Assuming Poisson statistics, the probability of detecting at least one event would be 0.15, 0.55 and 0.80 after 1, 5 and 10 yr respectively in the Virgo cluster alone. While the spatial distribution of the dEn galaxies in the Coma cluster has apparently not been determined, we expect higher overall rates in Coma than in Virgo due to its greater richness.

Some tidal flaring models (Gurzadyan & Ozernoy 1980, Cannizzo, Lee, & Goodman 1990) predict that single flares should persist for as long as several months or years, and inspection of the light curves of the handful of candidate X-ray events (Komossa & Dahlem 2002) suggests decay times of this order. Such long decay times would imply a non-trivial probability of observing an ongoing disruption event *somewhere* in the Virgo or Coma cluster at any given time. Non-detection of X-ray flares in these clusters would constitute robust evidence that dE galaxies do not harbor IMBHs.

7. CONCLUSIONS

1. In most galaxies, the predicted rate of stellar tidal disruptions varies inversely with assumed black hole mass. This is particularly true for galaxies with steep central density profiles, which dominate the overall event rate.
2. The downward revision in black hole masses that followed the discovery of the $M_{\bullet} - \sigma$ relation implies a total flaring rate per unit volume that is about an order of magnitude higher than in earlier studies.
3. An accurate analytic expression (equation 29) can be derived that gives the tidal flaring rate as a function of black hole

mass and stellar velocity dispersion in galaxies with $\rho \propto r^{-2}$ nuclei.

4. If black holes are present in nucleated spheroids fainter than $M_V \approx -19$, the tidal disruption rate due to dwarf galaxies in the Virgo cluster would be of order 0.2 yr^{-1} . Non-detection of flares after a few years of monitoring would argue against the existence of intermediate mass black holes in dwarf galaxies.

We thank B. Binggeli, H. Cohn, A. Graham, M. Milosavljevic, C. Pryor, and M. Stiavelli for useful discussions. This work was supported by NSF grants AST 00-71099 and AST02-0631 and by NASA grants NAG5-6037 and NAG5-9046.

REFERENCES

- Balcells, M., Dominguez-Palmero, L. & Graham, A. 2001, in ASP Conf. Ser. 249, The Central Kiloparsec of Starbursts and AGN, ed. J. H. Knapen et al. (San Francisco: ASP), 167
- Balcells, M., Graham, A. W., Dominguez-Palmero, L. & Peletier, R. 2003, *ApJ*, 582, L79
- Binggeli, B., Sandage, A., & Tamman, G. A. 1985, *AJ*, 90, 1681
- Cannizzo, J. K., Lee, H. M., & Goodman, J. 1990, *ApJ*, 351, 38
- Carollo, C. M., Stiavelli, M., Seigar, M., de Zeeuw, P. T. & Dejonghe, H. 2002, *ApJ*, 123, 159
- Cohn, H., & Kulsrud, R. M. 1978, *ApJ*, 226, 1087 (CK)
- Donley, J. L., Brandt, W. N., Eracleous, M., & Boller, Th. 2002, *AJ*, 124, 1308
- Erwin, P., Graham, A. W. & Caon, N. 2003, preprint (astro-ph/0212335)
- Evans, C. R. & Kochanek, C. S. 1989, *ApJ*, 346, L13
- Faber, S. M. et al. 1997, *AJ*, 114, 1771
- Ferguson, H. C., & Binggeli, B. 1994, *Astron. Ap. Rev.* 6, 67
- Ferguson, H. C., & Sandage, A. 1989, *AJ*, 346, L53
- Ferguson, H. C., & Sandage, A. 1991, *AJ*, 101, 765
- Ferrarese, L., & Merritt, D. 2000, *ApJ*, 539, L9
- Filippenko, A., & Ho, L. C. 2003, preprint (astro-ph/0303429)
- Frank, J., & Rees, M. J. 1976, *MNRAS*, 176, 633 (FR)
- Freeman, K. 1993, in ASP Conf. Ser. 48, The Globular Cluster-Galaxy Connection, ed. G. H. Smith & J. P. Brodie (San Francisco: ASP), 608
- Gebhardt, K. et al. 1996, *AJ*, 112, 105
- Gebhardt, K. et al. 2000, *ApJ*, 539, L13
- Genzel, R. et al. 2003, preprint (astro-ph/0305423)
- Gezari, S., Halpern, J. P., Komossa, S., Grupe, D., & Leighly, K. M. 2003, preprint (astro-ph/0304063)
- Graham, A. W. & Guzman, R. 2003, preprint (astro-ph/0303391)
- Gurzadyan, V. G. & Ozernoy, L. M. 1980, *AA*, 86, 315
- Jerjen, H. & Binggeli, B. 1997, in The Nature of Elliptical Galaxies, ASP Conf. Ser. Vol. 116, ed. M. Arnaboldi, G. S. Da Costa, & P. Saha (San Francisco: ASP), 239
- Hills, J. G. 1975, *Nature*, 254, 295
- Kim, S. S., Park, M.-G., & Lee, H. M. 1999, *ApJ*, 519, 647
- Komossa, S. 2002, *Rev. Mod. Astron.* 15, 27
- Komossa, S., & Dahlem, M. 2002, preprint (astro-ph/0106422)
- Kormendy, J. & Gebhardt, K. 2001, *AIP Conf. Proc.* Vol. 586, ed. J. C. Wheeler & H. Martel, 363
- Lauer, T. et al. 1998, *AJ*, 116, 2263
- Lidskii, V. V. & Ozernoi, L. M. 1979, *Pis'ma Astron. Zh.* 5, 28
- Magorrian, J., et al. 1998, *AJ*, 115, 2285
- Magorrian, J., & Tremaine, S. 1999, *MNRAS*, 309, 447 (MT)
- McLure, R. J. & Dunlop, J. S. 2002, *MNRAS*, 331, 795
- Merritt, D. 2003, preprint (astro-ph/0301257)
- Merritt, D., & Ferrarese, L. 2001a, *MNRAS*, 320, L30
- Merritt, D., & Ferrarese, L. 2001b, in ASP Conf. Ser. 249, The Central Kiloparsec of Starbursts and AGN: The La Palma Connection, ed. H. Knapen, J. E. Beckman, I. Shlosman, & T. J. Mahoney. (San Francisco: ASP), 335
- Merritt, D. & Fridman, T. 1996, in ASP Conf. Ser. 86, Fresh Views of Elliptical Galaxies, ed. A. Buzzoni, A. Renzini, & A. Serrano (San Francisco: ASP), 13
- Milosavljevic, M. & Merritt, D. 2003, preprint (astro-ph/0212459)
- Möllenhoff, C. & Heidt, J. 2001, *A&A*, 368, 16
- Peebles, P. J. E. 1972, *ApJ*, 178, 371
- Rees, M. J. 1988, *Nature*, 333, 523
- Rees, M. J. 1998, in Black Holes and Relativistic Stars, ed. R. M. Wald (Chicago: University of Chicago Press), 79
- Richstone, D. O. et al. 1998, *Nature*, 395, A14
- Sandage, A., Binggeli, B., & Tamman, G. A. 1985, *AJ*, 90, 1759
- Secker, J. & Harris, W. E. 1996, *ApJ*, 469, 623
- Spitzer, L. & Hart, M. H. 1971, *ApJ*, 164, 399
- Spitzer, L. & Harm, R. 1958, *ApJ*, 127, 544
- Stiavelli, M., Miller, B. W., Ferguson, H. C., Mack, J., Whitmore, B. C., & Lotz, J. M. 2001, *AJ*, 121, 1385
- Syer, D., & Ulmer, A. 1999, *MNRAS*, 306, 35 (SU)
- Trentham, N. & Tully, R. B. 2002, *MNRAS*, 335, 712
- Ulmer, A. 1999, *ApJ*, 514, 180
- van den Bergh, S. 1986, *AJ*, 91, 271
- van der Marel, R. 2003, preprint (astro-ph/0302101)
- Wandel, A. 1999, *ApJ*, 519, 39
- Young, P. 1980, *ApJ*, 242, 1232

TABLE 2
PREDICTED EVENT RATES DUE TO DWARF GALAXIES

Name	Rate ($\text{yr}^{-1} \text{ Mpc}^{-2}$)
Coma cluster	0.093
Virgo cluster	0.11
NGC 1407 group	0.057
Coma I	0.032
Leo group	0.0063
NGC 1023 group	0.027
Ursa Major group	0.0079

TABLE 1
GALAXY SAMPLE^a

Name	Profile ^b	Distance (Mpc)	$\log_{10}(r_b)$ (pc)	μ_b	α	β	Γ	Υ_V (M_\odot/L_\odot)	$\log_{10}(L_V/L_\odot)$	$\log_{10}(M_\bullet/M_\odot)^c$	$\log_{10}\dot{N}^d$ (yr^{-1})	$\log_{10}(M_\bullet/M_\odot)^e$	$\log_{10}\dot{N}^f$ (yr^{-1})
NGC221	\	0.8	-0.26	11.77	0.98	1.36	0.01	2.27	8.57	6.38	-3.79	6.32	-3.78
NGC224	\	0.8	0.11	13.44	4.72	0.81	0.12	26.1	9.86	7.79	-3.70	6.13	-3.56
NGC596	\	21.2	2.56	18.03	0.76	1.97	0.55	4.16	10.29	8.69	-5.01	7.69	-4.52
NGC1023	\	10.2	1.96	16.17	4.72	1.18	0.78	5.99	9.99	8.55	-4.46	8.17	-4.19
NGC1172	\	29.8	2.55	18.61	1.52	1.64	1.01	2.57	10.23	8.42	-4.75	6.90	-3.24
NGC1426	\	21.5	2.23	17.53	3.62	1.35	0.85	4.91	10.07	8.54	-4.87	7.50	-4.08
NGC3115	\	8.4	2.07	16.17	1.47	1.43	0.78	7.14	10.23	8.61	-4.19	8.74	-4.28
NGC3377	\	9.9	0.64	12.85	1.92	1.33	0.29	2.88	9.81	7.79	-4.16	7.51	-4.04
NGC3599	\	20.3	2.12	17.58	1.30	1.66	0.79	2.09	9.82	7.91	-5.24	6.22	-4.15
NGC3605	\	20.3	1.94	17.25	9.14	1.26	0.67	4.05	9.59	8.10	-5.17	6.76	-4.50
NGC4239	\	15.3	1.98	18.37	14.5	0.96	0.65	3.37	9.19	7.49	-5.57	5.69	-4.84
NGC4387	\	15.3	2.52	18.89	3.36	1.59	0.72	5.34	9.48	7.99	-5.13	6.83	-4.46
NGC4434	\	15.3	2.25	18.21	0.98	1.78	0.70	4.73	9.52	7.97	-4.81	6.81	-4.16
NGC4458	\	15.3	0.95	14.49	5.26	1.43	0.49	4.00	9.52	7.90	-4.58	6.78	-4.23
NGC4464	\	15.3	1.95	17.35	1.64	1.68	0.88	4.82	9.22	7.69	-4.21	7.26	-3.88
NGC4467	\	15.3	2.38	19.98	7.52	2.13	0.98	6.27	8.75	7.32	-4.48	6.04	-3.30
NGC4478	\	15.3	1.10	15.40	3.32	0.84	0.43	5.03	9.79	8.27	-5.00	7.34	-4.64
NGC4551	\	15.3	2.46	18.83	2.94	1.23	0.80	7.25	9.57	8.21	-4.96	7.11	-4.19
NGC4564	\	15.3	1.59	15.70	0.25	1.90	0.05	4.48	9.91	8.40	-4.67	7.71	-4.27
NGC4570	\	15.3	2.32	17.29	3.72	1.49	0.85	5.52	9.95	8.47	-4.49	8.01	-4.14
NGC4621	\	15.3	2.34	17.20	0.19	1.71	0.50	6.73	10.44	8.45	-4.04	8.49	-4.07
NGC4697	\	10.5	2.12	16.93	24.9	1.04	0.74	6.78	10.34	8.95	-5.03	7.73	-4.25
NGC4742	\	12.5	1.93	16.69	48.6	1.99	1.09	1.76	9.62	7.65	-3.80	6.85	-2.90
NGC5845	\	28.2	2.49	17.52	1.27	2.74	0.51	6.69	9.88	8.48	-4.56	8.70	-4.66
NGC7332	\	20.3	1.88	15.72	4.25	1.34	0.90	1.56	9.90	7.87	-4.33	7.21	-3.78
A2052	∩	132.0	2.43	18.36	8.02	0.75	0.20	12.80	11.00	9.88	-5.65	8.62	-4.90
NGC720	∩	22.6	2.55	17.50	2.32	1.66	0.06	8.15	10.58	9.27	-5.47	8.51	-5.50
NGC1399	∩	17.9	2.43	17.06	1.50	1.68	0.07	12.73	10.62	9.72	-5.22	9.08	-5.09
NGC1600	∩	50.2	2.88	18.38	1.98	1.50	0.08	14.30	11.01	10.06	-5.71	9.11	-5.62
NGC3379	∩	9.9	1.92	16.10	1.59	1.43	0.18	6.87	10.15	8.59	-4.90	8.30	-4.85
NGC4168	∩	36.4	2.65	18.33	0.95	1.50	0.14	7.54	10.64	9.08	-5.59	7.89	-5.47
NGC4365	∩	22.0	2.25	16.77	2.06	1.27	0.15	8.40	10.76	9.46	-5.29	8.57	-5.14
NGC4472	∩	15.3	2.25	16.66	2.08	1.17	0.04	9.20	10.96	9.42	-5.15	8.79	-5.05
NGC4486	∩	15.3	2.75	17.86	2.82	1.39	0.25	17.70	10.88	9.56	-5.35	9.16	-5.28
NGC4486b	∩	15.3	1.13	14.92	2.78	1.33	0.14	9.85	9.96	8.96	-4.84	8.17	-4.43
NGC4636	∩	15.3	2.38	17.72	1.64	1.33	0.13	10.40	10.60	8.36	-5.35	8.07	-5.37
NGC4649	∩	15.3	2.42	17.17	2.00	1.30	0.15	16.20	10.79	9.59	-5.19	9.19	-5.12
NGC4874	∩	93.3	3.08	19.18	2.33	1.37	0.13	15.00	11.35	10.32	-6.02	8.77	-5.91
NGC4889	∩	93.3	2.88	18.01	2.61	1.35	0.05	11.20	11.28	10.43	-5.81	9.20	-5.69
NGC5813	∩	28.3	2.04	16.42	2.15	1.33	0.08	7.10	10.66	9.29	-5.24	8.27	-5.10
NGC6166	∩	112.5	3.08	19.35	3.32	0.99	0.08	15.60	11.32	10.47	-6.16	8.84	-6.14
NGC524	∩	23.1	1.55	16.02	1.29	1.00	0.00	14.30	10.54	9.47	-	8.62	-
NGC1316	∩	17.9	1.55	14.43	1.16	1.00	0.00	2.56	11.06	9.25	-	8.36	-
NGC1400	∩	21.5	1.54	15.41	1.39	1.32	0.00	10.70	10.36	9.16	-	8.62	-
NGC1700	\	35.5	1.19	13.95	0.90	1.30	0.00	4.00	10.59	8.97	-	8.38	-
NGC2636	\	33.5	1.17	15.68	1.84	1.14	0.04	2.97	9.47	7.72	-	6.52	-
NGC2832	\	90.2	2.60	17.45	1.84	1.40	0.02	10.90	11.11	10.06	-	9.05	-
NGC2841	\	13.2	0.92	14.55	0.93	1.02	0.01	8.98	9.88	8.62	-	8.23	-
NGC3608	∩	20.3	1.44	15.45	1.05	1.33	0.00	7.04	10.27	8.39	-	8.01	-
NGC4552	∩	15.3	1.68	15.41	1.48	1.30	0.00	7.66	10.35	8.67	-	8.62	-
NGC7768	∩	103.1	2.30	16.99	1.92	1.21	0.00	9.51	11.10	9.93	-	8.82	-

^aAll parameters except for black hole mass and consumption rate are taken from Faber et al. (1997) and assume $H_0 = 80 \text{ km s}^{-1} \text{ Mpc}^{-1}$.

^bProfile class: ∩=core galaxy; \=power law galaxy

^cBlack hole mass from Magorrian et al. (1998).

^dConsumption rate based on the Magorrian et al. (1998) black hole mass.

^eBlack hole mass from the $M_\bullet - \sigma$ relation, equation (7).

^fConsumption rate based on the $M_\bullet - \sigma$ black hole mass.